Journal of Theoretical and Applied Information Technology
31st December 2021. Vol.99. No 24

ISSN: 1992-8645 www.jatit.org E-ISSN: 1817-3195

LINEAR MODEL OF BOOST CONVERTER WITH ACTIVE POWER FACTOR CORRECTION

[1]EDILBERTO CARLOS VIVAS, [2]EDWAR JACINTO GÓMEZ, [3]GABRIEL DE JESUS CAMARGO

[1,3]Facultad de Ingeniería, Universidad Libre, Bogotá, Colombia

[2]Facultad Tecnológica, Universidad Distrital Francisco José de Caldas, Bogotá, Colombia

E-mail: [1]edilbertoc.vivasg@unilibre.edu.co, [2]ejacintog@udistrital.edu.co, [3]gabriel.camargov@unilibre.edu.co

ABSTRACT

This paper describes the methodology for finding a Boost converter's linear mathematical model with active power factor correction. The linear model obtained is stable in an open-loop and contains a zero's located in the right half-plane. The Matlab-Simulink power electronics toolbox was used to verify that the linear model adequately represents the system dynamics around the operating point and that the power factor is close to unity. Otherwise, this article develops the complete model of the modulator-converter set in peak current mode; consider the disturbance generated by variations in the input voltage. In addition, the general scheme that allows the input current to the converter to have a sinusoidal waveform and correct the power factor is modeled. The total mathematical model obtained from the multiplier-modulator-converter set makes possible the design and implementation of different automatic control techniques.

Keywords: *Boost Converter, Power Factor Correction, State Space Model.*

1. INTRODUCTION

Power factor correction is a problem that is becoming increasingly relevant in small and medium-sized industries. Since their beginning, these companies have been in residential sectors with electrical installations that do not comply with requirements to handle reactive power Q. Therefore, this situation has required these companies to be oversize the electrical power capacity of the distribution transformers and the cable gauges used for transmission [1]. One alternative to reducing such reactive load is to interconnect capacitor banks or synchronous motors depending on the power factor value to be corrected [2], passive control strategies that in most cases bring additional problems. Another alternative is active control strategies, which increase power factor using active electronic circuits with feedback to change the drawn current.

In addition to the use in small industry and medium industry, there are several possible applications of converters with active power factor correction - Boost type [3], such as:

- rapid charging of battery banks [4][5],
- efficient use of solar panels or renewable energy sources [6],
- power supplies of non-linear high frequency or power systems [7],
- LED lighting loads [8].

These applications require mathematical models that take control signals and disturbances into account to design control algorithms that guarantee good performance and stability.

Within the different active control techniques of power factor are used mixed strategies. These use cascade AC-DC and DC-DC converters [9][10][11] that correct the problems to handle output voltage of the first stage using combinations of Boost and Fly-Back converters [6] to have manageable voltage levels at the output.

The industrial loads representing AC-DC converters are non-linear loads [12] that generate phase shifts regarding the input signal, and also they bring about surges, harmonic distortion, and electromagnetic interference [13]. For this reason, an active control strategy for the power factor (PF)

makes it possible to include these and many more variables that achieve increased system efficiency and lead to load significantly reduced on the energy distribution network.

Previous works analyze converters in peak current mode; in them, particular emphasis is made on the design of the compensation ramp for the internal current loop [14][15][10][16], guaranteeing the stability of a T-periodic orbit and avoiding subharmonic solutions.

Push-Pull, FlyBack, and Forward converters, among others, generate significant harmonic distortion and electromagnetic interference regarding the Boost type converter and its variations. For this reason, the Boost type converter is used for most classical control strategies and artificial intelligence techniques such as Fuzzy Logic [17] or Neural Networks. Also, this type of converter allows to increase the working frequency, make isolation with the load, and it can be combined with a Buck-Boost [18][4] so that with a suitable control strategy, the total harmonic distortion (THD) can be reduced [6][15].

Consequently, this article develops the complete model of the modulator-converter set in peak current mode, which considers the disturbance generated by variations in the input voltage. In addition, the general scheme that allows the input current to the converter to have a sinusoidal waveform and correct the power factor is modeled. The total mathematical model obtained from the multiplier-modulator-converter set makes possible the design and implementation of different automatic control techniques.

First, in the paper, the development of the Boost converter model is shown, considering the disturbance input due to input voltage variations and the control input, which is the pulse width of the PWM signal. Second, the modulator is modeled in peak current mode to obtain the transfer function of the converter output voltage versus the reference voltage of the modulator voltage comparator. Third, the multiplier circuit that allows the input current to the converter to be sinusoidal waveform and in phase with the input voltage to correct the power factor is analyzed. Finally, the Matlab-Simulink power electronics toolbox is used to compare the dynamics of the electrical circuit concerning the linear model obtained from the multiplier-modulator-converter assembly to demonstrate that the current in the coil is sinusoidal and that a power factor close to unity is obtained.

2. METHODS

The drive selected to perform the active power factor correction is the Boost topology drive in continuous operation mode. The Boost topology produces a higher output voltage than the input voltage; the electronic circuit is shown in figure 1. The converter operates in continuous mode when the current in the inductor never reaches zero; that is, it is maintained with a variation Δi_L small around a specific value. The Boost topology in continuous mode is favorable because as input current is continuous, it lets to have control in the current mode in all variations of the line voltage, even zero voltage.

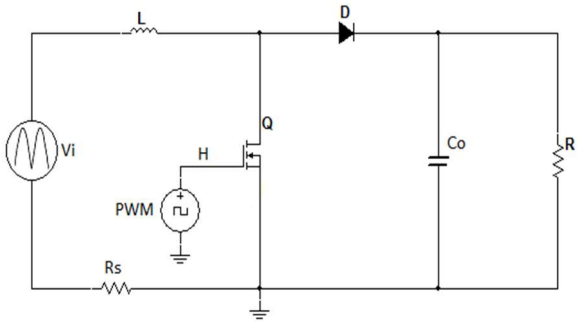

Figure 1: Boost Converter

The qualities of the Boost converter are [19]:

- The voltage on the switching transistor is never higher than the output voltage.
- The inductor at the input blocks transients from the network, and the output capacitor stores energy more efficiently.
- Easy handling of transistor gate activation to ground.

Figure 2 shows the operation of the Boost converter. When the transistor is ON, the coil stores energy through the source and the capacitor feeds the load with its stored energy, half-cycle a). When the transistor is OFF, the current flows through the diode, capacitor, and load, half-cycle b).

Journal of Theoretical and Applied Information Technology
31st December 2021. Vol.99. No 24

ISSN: 1992-8645 www.jatit.org E-ISSN: 1817-3195

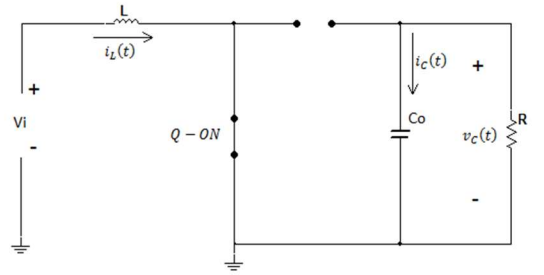

a) Transistor On

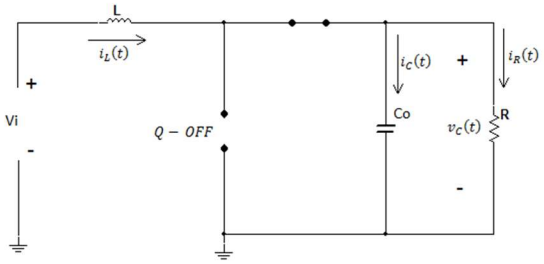

b) Transistor Off

Figure 2: Boost Converter Operating Semi-cycles

2.1 Linear Model of Boost Converter

Taking as a reference figure 2, when the switch is ON, the v_L and i_c are defined, as shown in equation 1.

$$v_L = L\frac{di_L}{dt} = v_i \quad ; \; i_c = C_o\frac{dv_c}{dt} = -\frac{v_c}{R} \tag{1}$$

However, V_L is equivalent to the difference of v_i and v_C when the switch is OFF, and i_c also changes, as shown in equation 2.

$$v_L = L\frac{di_L}{dt} = v_i - v_c \; ; \; i_c = C_o\frac{dv_c}{dt} = i_L - \frac{v_c}{R} \tag{2}$$

In a stationary state, i.e., at the equilibrium point, the v_C and the $i_L$are as shown in equation 3.

$$v_c = V\,(constant) \; ; \quad i_L = I\,(constant) \tag{3}$$

Figure 3 shows the waveform of v_L e i_C in the elements through time.

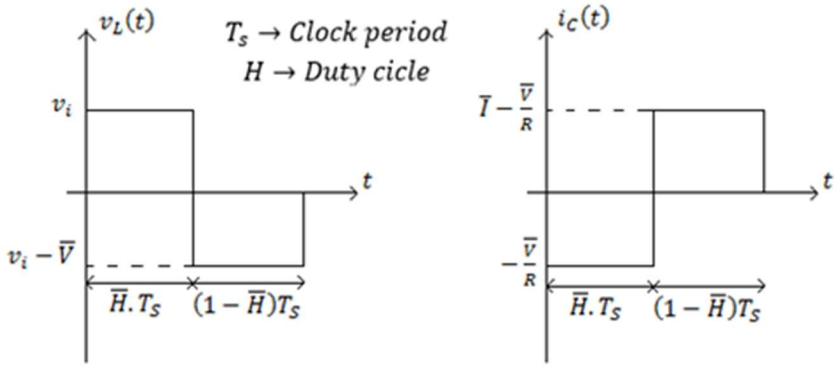

Figure 3: Signals in Elements

The average value of v_L and i_C is zero in steady-state in a switching period, from which state equations of the non-linear system are obtained, as shown in equation 4.

$$\frac{di_L}{dt} = \frac{H.v_i + (1-H)(v_i - V)}{L} = \frac{v_i - (1-H)V}{L}$$
$$\frac{dv_c}{dt} = \frac{-\frac{V}{R}H + (1-H)\left(I - \frac{V}{R}\right)}{C_o} = -\frac{V}{RC_o} + \frac{(1-H)I}{C_o} \tag{4}$$

When the system is in balance, the derivatives of the state variables are equal to zero; then the necessary pulse width $\bar{H}$ to obtain the desired output voltage $\bar{V}$ and the current in the balance coil $\bar{I}$ will be as presented in equation 5.

$$\frac{di_L}{dt} = \frac{\bar{v}_i - (1-\bar{H})\bar{V}}{L} = 0 \Rightarrow \bar{H} = 1 - \frac{\bar{v}_i}{\bar{V}}$$
$$\bar{v}_i = \frac{2\bar{v}_{ipeak}}{\pi}; \; \bar{I} = \frac{2i_{Lpeak}}{\pi} \tag{5}$$

Linearizing around the point of balance induced by $\bar{H}$, $\bar{V}$ and $\bar{I}$, are obtained equation 6.

$$\begin{bmatrix} \frac{d\hat{\imath}_L}{dt} \\ \frac{d\hat{v}_c}{dt} \end{bmatrix} = \begin{bmatrix} 0 & \frac{-(1-\bar{H})}{L} \\ \frac{1-\bar{H}}{C_o} & -\frac{1}{RC_o} \end{bmatrix} \begin{bmatrix} \hat{\imath}_L \\ \hat{v}_c \end{bmatrix} + \begin{bmatrix} \frac{1}{L} & \frac{\bar{V}}{L} \\ 0 & -\frac{\bar{I}}{C_o} \end{bmatrix} \begin{bmatrix} \hat{v}_i \\ \hat{H} \end{bmatrix} \quad (6)$$

Where:

$\hat{\imath}_L = i_L - \bar{I}$; $\hat{v}_c = v_c - \bar{V}$; $\hat{v}_i = v_i - \bar{v}_i$;

$$\hat{H} = H - \bar{H}$$

Therefore, the output equation is shown in equation 7.

$$\begin{bmatrix} Y_1 \\ Y_2 \end{bmatrix} = \begin{bmatrix} 0 & 1 \\ 1 & 0 \end{bmatrix} \begin{bmatrix} \hat{\imath}_L \\ \hat{v}_c \end{bmatrix} + \begin{bmatrix} 0 & 0 \\ 0 & 0 \end{bmatrix} \begin{bmatrix} \hat{v}_i \\ \hat{H} \end{bmatrix} \quad (7)$$

It is important to note that the drive control signal is the duty cycle "H", and input voltage variations "vi ", are seen as a disturbance input.

2.2 PWM Modulator Model

The circuit converter in the mode of peak current has two feedback loops. The external loop of voltage keeps the output voltage constant, and it produces the reference V_{ref} for the internal loop of current, which generates the PWM signal that controls the turning on of the transistor. The internal loop of current transforms the coil and the switch into a controlled current source, reducing the system's dynamic model in one order. Furthermore, it avoids overcurrents in the semiconductor during supply voltage transients and loads variations because the peak current is controlled in each switching cycle.

Figure 4 shows the diagram of the Boost converter with the PWM modulator circuit. At the beginning of the switching cycle, the oscillator clock sets the output of RS bistable to "1", which turns the transistor on. Then, when the voltage at the sensor resistor R_s plus the compensation ramp voltage slightly exceeds the reference voltage V_{ref}, the output of the comparator changes to "1" and the bistable changes to "0", which turns the transistor off.

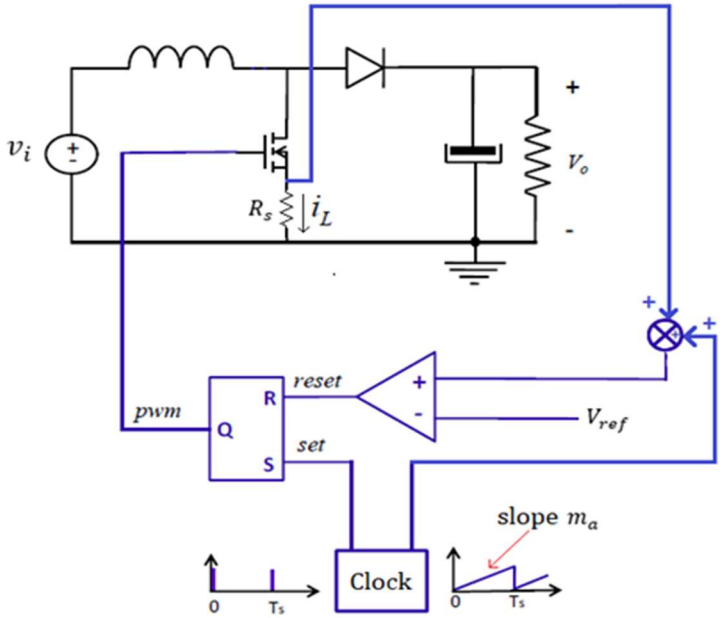

Figure 4: Control Mode of Boost Converter by Peak Current

A compensation ramp is required (m_a) because, without this signal, the duty cycle of the modulator for $\bar{H} > 0.5$ does not remain stable in case of disturbances; the reason is that the coil discharge time is insufficient to reach in a finite number of cycles the initial load value of this [20]. Figure 5 shows the signals waveforms of the internal loop of current.

For each switching semi-cycle ON and OFF of the transistor, an expression gets as shown in equation 8.

$$\underbrace{L.\frac{\Delta i_L}{HT_s}}_{m_1}.R_s = R_s.\bar{v}_i \; ; \qquad \underbrace{L.\frac{\Delta i_L}{(1-H)T_s}}_{m_2}.R_s = R_s(\bar{v}_i - \bar{V}) \qquad (8)$$

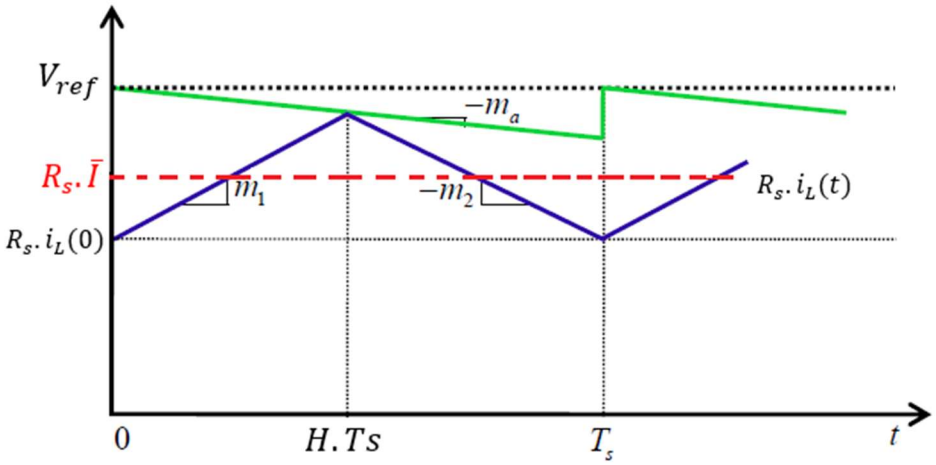

Figure 5: Signals Waveforms of Internal Loop of Current

According to figure 4 and figure 5 above, it can see that the voltage comparator switches every time what is expressed in equation 10 is fulfilled.

$$\left(\bar{I} + \frac{\Delta {i_L}^+}{2}\right).R_s + m_a.\bar{H}.T_s = \bar{V}_{ref} \qquad (10)$$

$$\Delta {i_L}^+ = \frac{\bar{v}_i}{L}.\bar{H}.T_s$$

$$\bar{I} = \frac{\bar{V}_{ref}}{R_s} - \left(\frac{2L.m_a.T_s + \bar{v}_i R_s.T_s}{2L.R_s}\right)\bar{H}$$

Linearizing around the point of balance gets equation 11.

$$\partial\bar{I} = \frac{\partial\bar{I}}{\partial V_{ref}}\partial V_{ref} + \frac{\partial\bar{I}}{\partial v_i}\partial v_i + \frac{\partial\bar{I}}{\partial H}\partial H \qquad (11)$$

A value usually assigned for the compensation ramp is presented in equation 9.

$$m_a = \frac{|m_2|}{2} \qquad (9)$$

$$\partial\bar{I} = \frac{1}{R_s}\partial V_{ref} - \frac{HT_s}{2L}\partial v_i - \left(\frac{2L.m_a.T_s + v_i R_s.T_s}{2L.R_s}\right)\partial H$$

At clearing the equation before, it gets equation 12.

$$\partial H = \frac{2L}{2L.m_a.T_s + \bar{v}_i R_s.T_s}\partial V_{ref} - \frac{2L.R_s}{2L.m_a.T_s + \bar{v}_i R_s.T_s}\partial\bar{I} - \frac{R_s\bar{H}}{2L.m_a + \bar{v}_i R_s}\partial v_i \qquad (12)$$

$$\partial H = G_{V_{ref}}.\partial V_{ref} - G_I.\partial\bar{I} - G_{v_i}.\partial v_i$$

Then, the transfer function block diagram of the modulator-converter assembly can be seen in Figure 6.

Journal of Theoretical and Applied Information Technology
31st December 2021. Vol.99. No 24

ISSN: 1992-8645 www.jatit.org E-ISSN: 1817-3195

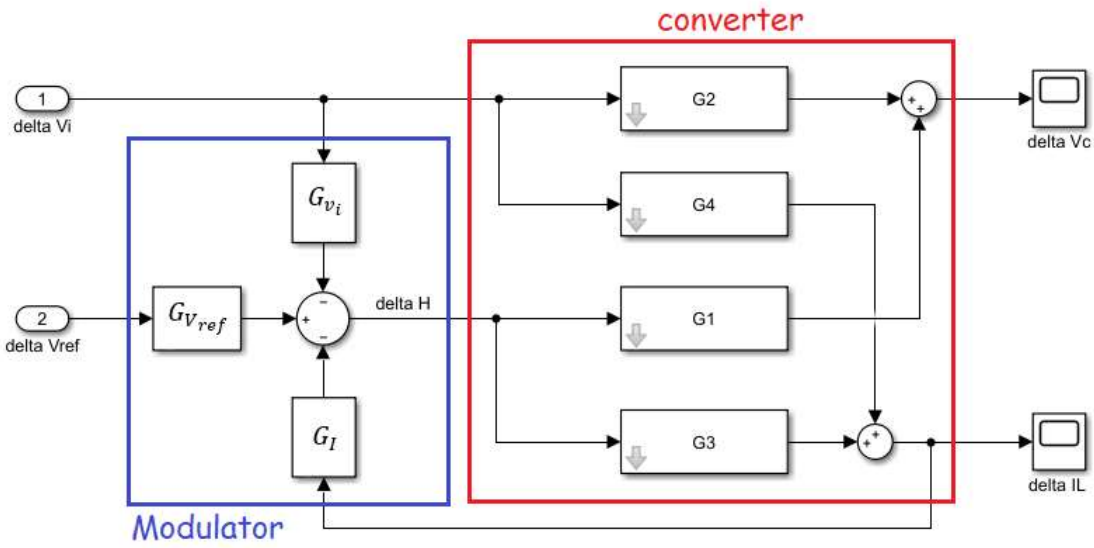

Figure 6: Block Diagram of Modulator-Converter Assembly

In equation 13, the general transfer functions of blocks G1, G2, G3, and G4 are presented.

$$G1 = \frac{v_c(s)}{H(s)} \;\; ; \;\; G2 = \frac{v_c(s)}{v_i(s)}$$
$$G3 = \frac{i_L(s)}{H(s)} \;\; ; \;\; G4 = \frac{i_L(s)}{v_i(s)} \qquad (13)$$

Therefore, in equation 14, the transfer function $\frac{i_L(s)}{V_{ref}(s)}$ considering $\Delta v_i = 0$ by overlay is shown.

$$\frac{i_L(s)}{V_{ref}(s)} = \left(G_{V_{ref}}\right)\left(\frac{G3}{1 + \underbrace{G_I.G3}_{\gg 1}}\right) \approx \frac{G_{V_{ref}}G3}{G_I.G3} \qquad (14)$$
$$\frac{i_L(s)}{V_{ref}(s)} = \frac{G_{V_{ref}}}{G_I} = \frac{1}{R_s}$$

It is demonstrated that the inner loop is transformed into a controlled current source with a gain of $\frac{1}{R_s}$, i.e., if the waveform of $V_{ref}(s)$ is sinusoidal, the current waveform will also be sinusoidal. For the external loop of voltage, by considering voltage variations Δv_i as a disturbance, it gets equation 15.

$$\frac{v_c(s)}{V_{ref}(s)} = \left(G_{V_{ref}}\right)\left(\frac{1}{1 + \underbrace{G_I.G3}_{\gg 1}}\right)G1 \qquad (15)$$
$$\frac{v_c(s)}{V_{ref}(s)} \approx \frac{G_{V_{ref}}.G1}{G_I.G3} = \frac{1}{R_s}.\frac{G1}{G3}$$

$$\boxed{\frac{v_c(s)}{V_{ref}(s)} = \frac{Ls + R(2\bar{H} - 1 - \bar{H}^2)}{C_o.R.R_s(\bar{H} - 1)s + (2\bar{H} - 2)R_s} = G_T(s)}$$

2.3 Total Block Diagram for Power Factor Correction

Correcting the power factor consists of making the voltage and current signal in phase and have the same waveform, i.e., the power network "sees" the load is purely resistive, achieving a unitary power factor. The input voltage to the Boost converter is a full-wave rectified signal "unfiltered". The resistance R_s (small value) allows sensing the current level in L, which is the same supply network current.

Thus, in order for the current $i_L(t)$ to be sinusoidal and is in phase with the input voltage, a signal is generated v_x from the rectified input voltage. That signal is multiplied with the control signal u so that the reference signal V_{Ref} has the same input voltage waveform and is in phase with it. Figure 7 shows the overall block diagram.

The current in the coil will have the same waveform as the input voltage, as the internal loop of current ensures tracking. The values of L and C_o must be chosen appropriately so that the output loop of voltage and the ΔI_L are small; it is usually designed so that $\Delta I_L \cong 0.05\bar{I}$. Multiplying the control signal u by $v_x(t)$ is equivalent to multiplying u by the average value of the signal $v_x(t)$ because the converter behaves like a low-pass filter that blocks the passage of the fundamental frequency and the harmonics of the rectified signal $v_x(t)$. The average value of $v_x(t)$ is presented in equation 16.

$$v_{xavg} = \frac{2v_{xpeak}}{\pi} = \frac{2K_{div}.\bar{v}_{ipeak}}{\pi} \quad (16)$$

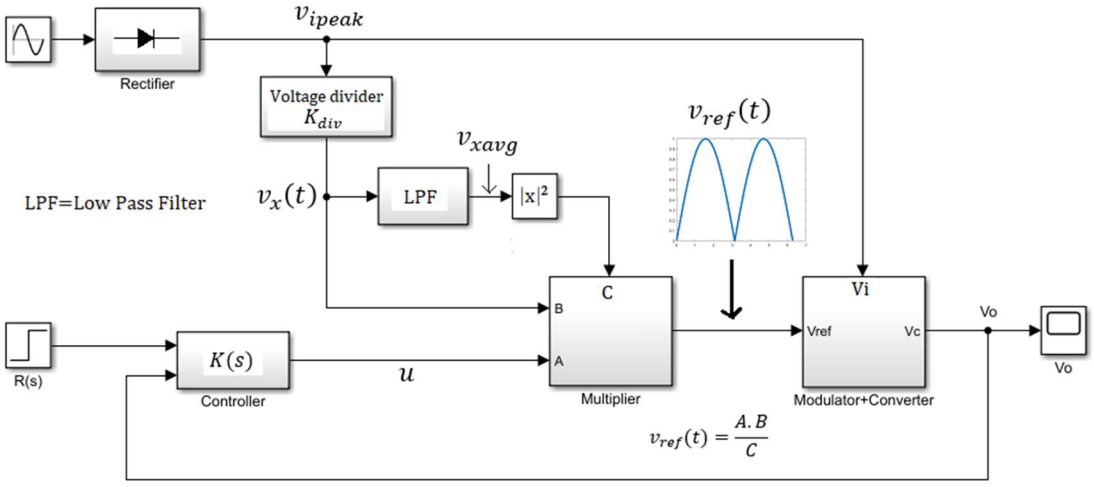

Figure 7: Total Block Diagram for Power Factor Correction

The low pass filter (LPF) extracts only the average level of $v_x(t)$. Input "C" is the divider input that generates feedforward control action. This input is proportional to the average square $v_x(t)$ and adjusts the multiplier's gain to maintain constant voltage loop gain in the face of input voltage variations. If the input voltage v_i then decreases, $v_x(t)$ also decreases. However, the current loop reference voltage v_{ref} increases the input peak current (i_{Lpeak}) and tries to keep the output voltage constant.

From the block diagram in Figure 7, equation 17 is obtained.

$$\bar{V}_{ref} = \frac{u\,.\,v_{xavg}}{{v_{xavg}}^2} = \frac{\bar{u}}{\bar{v}_{xavg}} = \frac{\bar{u}.\pi}{2K_{div}.\bar{v}_{ipeak}} \quad (17)$$

Linearizing around the point of balance induced by $\bar{v}_{ipeak}$ and the balance control signal $\bar{u}$, equation 18 is getting.

$$\partial V_{ref} = \frac{\partial V_{ref}}{\partial u}\partial u + \frac{\partial V_{ref}}{\partial v_{ipeak}}\partial v_{ipeak} \quad (18)$$

$$\partial V_{ref} = \frac{\pi}{2K_{div}.\bar{v}_{ipeak}}\partial u - \frac{\bar{V}_{ref}}{\bar{v}_{ipeak}}\partial v_{ipeak}$$

Then, the linear model in the face of variations of v_i and the control signal u can be seen in Figure 8.

Journal of Theoretical and Applied Information Technology
31st December 2021. Vol.99. No 24

ISSN: 1992-8645 www.jatit.org E-ISSN: 1817-3195

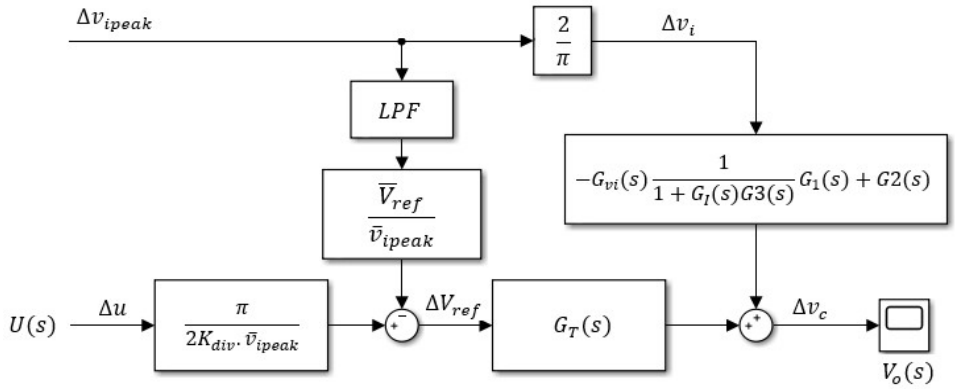

Figure 8: Voltage Loop Model

Finally, the total model of the voltage loop of the power factor correction converter used to design the output voltage controller is presented in equation 19.

$$\frac{V_o(s)}{U(s)} = \frac{\pi}{2K_{div}.\bar{v}_{ipeak}} G_T(s) \quad (19)$$

3. RESULTS AND DISCUSSION

The MATLAB-Simulink power electronics toolbox was used to compare the dynamics of the electrical circuit concerning the linear model, as shown in Figure 9 and Figure 10.

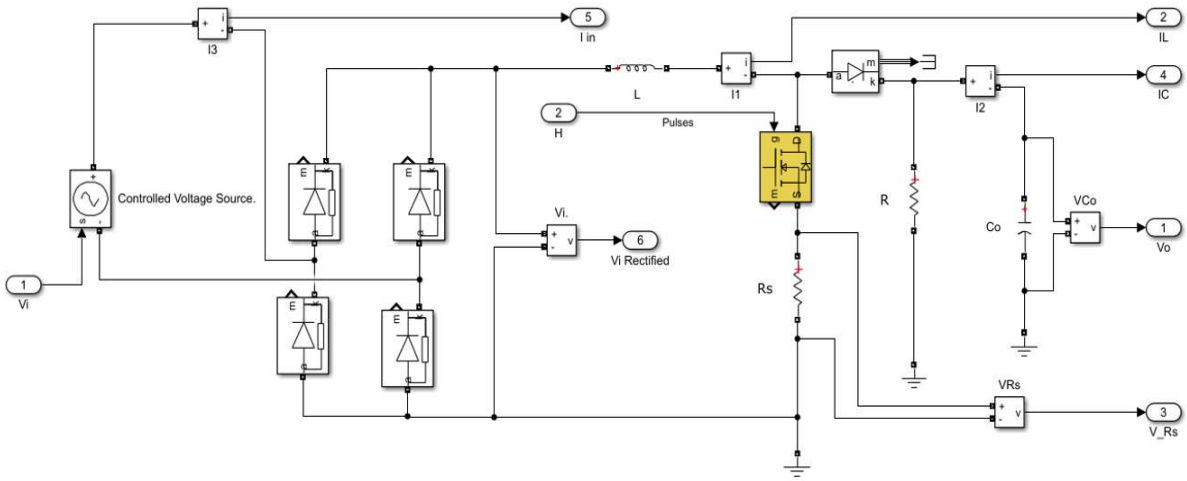

Figure 9: Boost Converter

Journal of Theoretical and Applied Information Technology
31st December 2021. Vol.99. No 24

ISSN: 1992-8645 www.jatit.org E-ISSN: 1817-3195

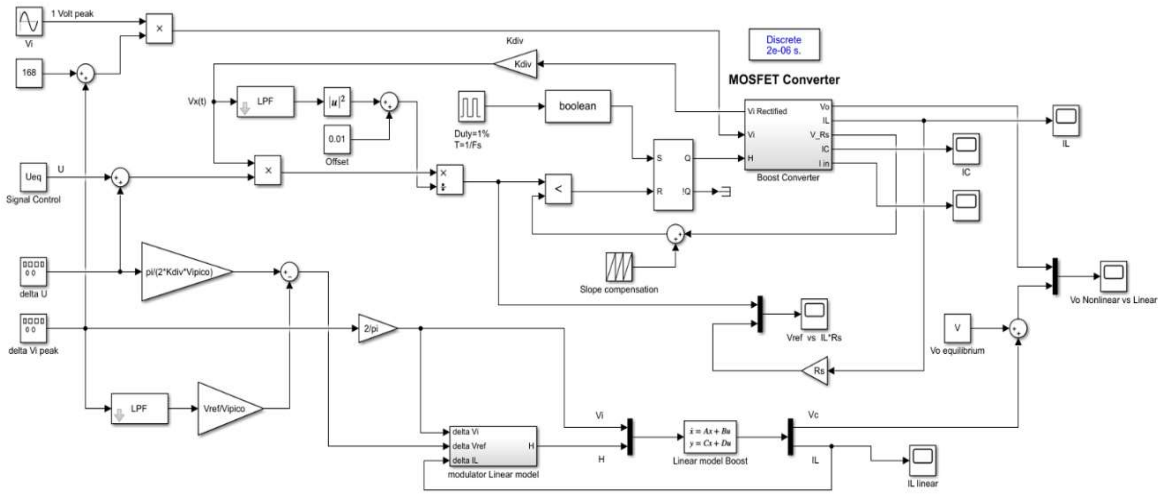

Figure 10: Boost PFC vs Linear System

The design conditions can be seen in table 1.

Table 1: Design Equations

$\bar{V} = 400\ volts\ ;$ $P = 800\ watts$	$I_{peak} = \frac{\sqrt{2}.P}{V_{irms}}$	$L = \frac{\bar{v}_i.\bar{H}.T_s}{\Delta i_L}$	$m_2 = \frac{R_s(\bar{v}_i - \bar{V})}{L}$
$R = \frac{V^2}{P}\ ohms$	$\bar{v}_i = \frac{2v_{ipeak}}{\pi}$	$T_{v_i} = 1/120Hz$	$m_a = \frac{\lvert m_2 \rvert}{2}$
$T_s = 1/50KHz$	$\bar{H} = 1 - \frac{\bar{v}_i}{\bar{V}}$	$\Delta V_o = 0.05\bar{V}$	$\bar{V}_{ref} = \left(\bar{I} + \frac{\Delta i_L}{2}\right) R_s + m_a.\bar{H}.T_s$
$v_{ipeak} = 168\ volts\ peak$	$\bar{I} = \frac{2I_{peak}}{\pi}$	$C_o = \frac{\bar{V}.\bar{H}.T_{v_i}}{2.R.\Delta V_o}$	$v_{xavg} = 2\ volts\ ;$ $K_{div} = \frac{v_{xavg}}{v_{iavg}}$
$v_{irms} = \frac{v_{ipeak}}{\sqrt{2}}$	$\Delta i_L = 0.05\bar{I}$	$R_s = 0.33\ ohms$	$\bar{u} = \bar{V}_{ref}.v_{xavg}$

The Balance control signal is applied ($\bar{u}$) to bring the system to the desired balance point ($\bar{V}$) and a slight variation is generated around the equilibrium point to check that the dynamic response of the two systems is similar, as shown in Figure 11 and Figure 12.

The system is shown to reject input peak voltage variations (Δv_{ipeak}); it allows the gain of the voltage loop to be kept constant.

Journal of Theoretical and Applied Information Technology
31st December 2021. Vol.99. No 24

ISSN: 1992-8645 www.jatit.org E-ISSN: 1817-3195

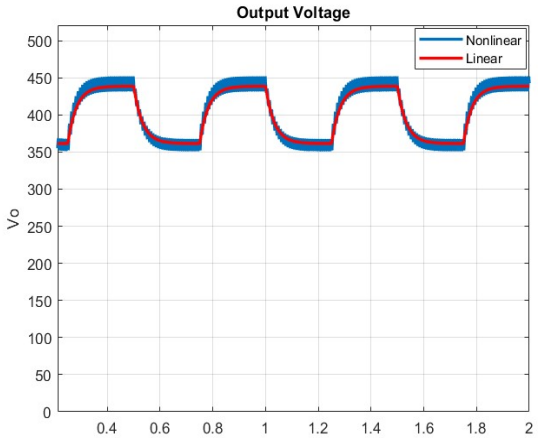

Figure 11: Output Voltage for $\Delta u = \pm 0.2\bar{u}$

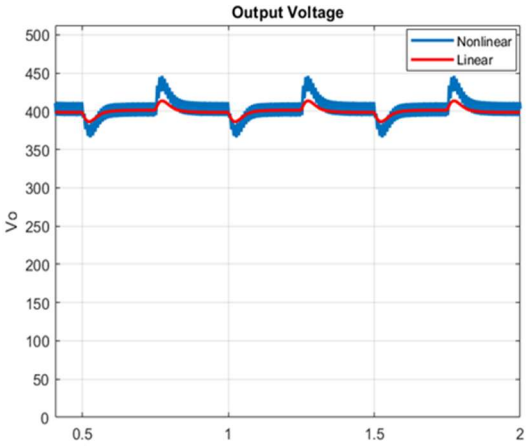

Figure 12: Output Voltage for $\Delta v_{ipeak} = \pm 0.1\bar{v}_{ipeak}$

Figure 13 shows the response of the internal loop of current. The current $i_L(t)$ follows the reference signal obtaining a power factor close to the unit, which is the objective of this work.

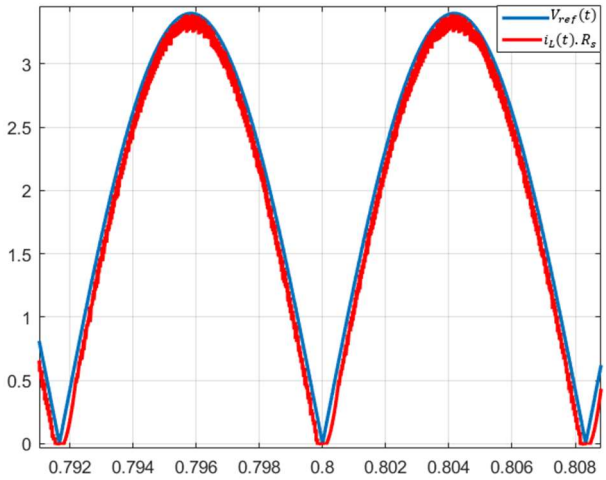

Figure 13: Current in the $i_L(t).R_s$ *vs* $V_{ref}(t)$

The PF is affected by the phase shift between line voltage and the line current, also by the harmonic distortion in source current. Total Harmonic Distortion (THD) can be obtained as shown in equation 20.

$$THD = \frac{\sqrt{\sum_{n=2}^{\infty} {I_n}^2}}{I_1} 100\% \qquad (20)$$

I_1 is the magnitude of the fundamental frequency (60Hz) and I_n is the magnitude of the harmonics. Calculating THD the input current signal with a sampling frequency of 500KHz, a THD=4.62% was obtained, as shown in Figure 14.

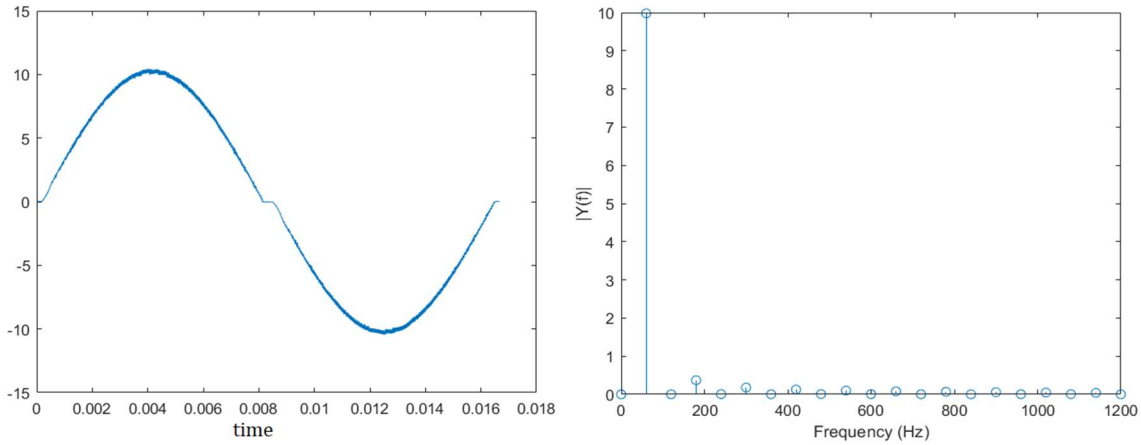

Figure 14: Single-Sided Amplitude Spectrum of $i_L(t)$ for 20 Harmonics

4. CONCLUSIONS

The linear mathematical model of the Boost converter with active power factor correction, developed in this article, adequately represents the system's dynamics around the point of operation.

It was demonstrated that the internal loop of current is transformed into a controlled current source. The linear model obtained from the external loop of voltage is a first-order stable open-loop system, with a zero located in the right half-plane.

The simulation results show that the scheme used generates a power factor close to the unit and has low harmonic distortion. The feed-forward control rejects input voltage variations and maintains constant voltage loop gain to improve system stability.

The state of the art reviewed in this paper shows that the models of the converter topologies are generally obtained. However, the total transfer function of the scheme used for active power factor correction is not evident. Since the total transfer function of the system is not available, it becomes difficult to replicate the results and design control algorithms for the voltage loop.

This work obtained the total transfer function of the voltage outer loop of the multiplier-modulator-converter set. With this model in future works could be possible to design different control strategies to achieve specific performance and stability characteristics under the variation of parameters such as system load and input voltage variations.

This work did not design the closed-loop control algorithm that maintains the output voltage stable under input voltage variations and converter load variations. Future work should analyze the change of the total converter model with active power factor correction under load variations to ensure the stability of the closed-loop system.

REFRENCES

[1] I. M. Safwat and W. Xiahua, "Comparative study between passive PFC and active PFC based on Buck-Boost conversion," *Proc. 2017 IEEE 2nd Adv. Inf. Technol. Electron. Autom. Control Conf. IAEAC 2017*, no. 1, pp. 45–50, 2017, doi: 10.1109/IAEAC.2017.8053974.

[2] C. A. Heger and A. Morroni, "Power Factor Correction-A Fresh Look into Today´s Electrical Systems," vol. 255, pp. 1–13, 2012.

[3] A. Vadde, S. Sachin, and V. V. S. N. SitaramGupta, "Real implementation of synchronous boost converter with controller for power factor correction," *TENSYMP 2017 - IEEE Int. Symp. Technol. Smart Cities*, pp. 23–26, 2017, doi: 10.1109/TENCONSpring.2017.8070061.

[4] C. P. Mehta and P. Balamurugan, "Buck-Boost converter as power factor correction controller for plug-in electric vehicles and battery charging application," *2016 IEEE 6th Int. Conf. Power Syst. ICPS 2016*, 2016, doi: 10.1109/ICPES.2016.7584111.

[5] P. Akter, M. Uddin, M. M. Rahman, M. Islam, and M. R. B. Bhuiyen, "Efficiency improvement of semi-bridgeless phase-shifted boost converter

with power factor correction in energy storage system," *2013 Int. Conf. Electr. Inf. Commun. Technol. EICT 2013*, pp. 1–5, 2014, doi: 10.1109/EICT.2014.6777836.

[6] M. W. Bin Mahmud, A. Z. Alam, and D. A. Rahman, "Improvement of Active Power Factor Correction Circuit for Switch Mode Power Supply Using Fly Back and Boost Topology," *Proc. 2018 7th Int. Conf. Comput. Commun. Eng. ICCCE 2018*, pp. 437–440, 2018, doi: 10.1109/ICCCE.2018.8539335.

[7] A. P. Ambade *et al.*, "Direct power control PWM Rectifier using Switching table for series resonant converter capacitor charging pulsed power supply," *2016 IEEE Int. Conf. Recent Trends Electron. Inf. Commun. Technol. RTEICT 2016 - Proc.*, pp. 758–762, 2017, doi: 10.1109/RTEICT.2016.7807928.

[8] J. E. Leal, "Diseño y construccion de un convertidor electronico para un arreglo de leds de 70 vatios de potencia," *Rev. la Fac. Med.*, vol. 26, no. 4, pp. 219–227, 2010.

[9] K. Chatterjee, S. Gupta, P. K. Saha, and A. Ghosh, "Exploration of nonlinear phenomena in Power-Factor-Correction boost converter," *2016 Int. Conf. Comput. Power, Energy, Inf. Commun. ICCPEIC 2016*, pp. 499–504, 2016, doi: 10.1109/ICCPEIC.2016.7557285.

[10] H. Coral-Enriquez, G. A. Ramos, and J. Cortes-Romero, "Power factor correction and harmonic compensation in an active filter application through a discrete-time active disturbance rejection control approach," *Proc. Am. Control Conf.*, vol. 2015-July, pp. 5318–5323, 2015, doi: 10.1109/ACC.2015.7172170.

[11] Z. Yu, M. Han, H. Wu, and Y. Xing, "A quasi single-stage power factor correction converter based on a three-level boost converter," *Proc. IECON 2017 - 43rd Annu. Conf. IEEE Ind. Electron. Soc.*, vol. 2017-Janua, pp. 669–674, 2017, doi: 10.1109/IECON.2017.8216116.

[12] J. Miret, M. Castilla, L. G. De Vicuna, P. Martí, and M. Velasco, "Non-linear control of a power-factor-correction rectifier with fast dynamic response," *IEEE Int. Symp. Ind. Electron.*, vol. 2016-Novem, pp. 504–509, 2016, doi: 10.1109/ISIE.2016.7744941.

[13] H. S. Nair and N. Lakshminarasamma, "Challenges in achieving high performance in boost PFC converter," *2017 IEEE Int. Conf. Signal Process. Informatics, Commun. Energy Syst. SPICES 2017*, 2017, doi: 10.1109/SPICES.2017.8091329.

[14] J. G. Muñoz, G. Gallo, F. Angulo, and G. Osorio, "Slope compensation design for a peak current-mode controlled boost-flyback converter," *Energies*, vol. 11, no. 11, pp. 1–18, 2018, doi: 10.3390/en11113000.

[15] O. Pop, G. Chindris, A. Grama, and F. Hurgoi, "Power factor correction circuit with a new modified SEPIC converter," *Proc. Int. Spring Semin. Electron. Technol.*, vol. 2001-Janua, pp. 117–120, 2001, doi: 10.1109/ISSE.2001.931026.

[16] D. M. Beams and S. Boppana, "Small-signal modeling of boost power-factor correction controllers," *Midwest Symp. Circuits Syst.*, pp. 1025–1028, 2010, doi: 10.1109/MWSCAS.2010.5548816.

[17] S. Arya Krishna and L. Abraham, "Boost converter based power factor correction for single phase rectifier using fuzzy logic control," *2014 1st Int. Conf. Comput. Syst. Commun. ICCSC 2014*, no. December, pp. 122–126, 2003, doi: 10.1109/COMPSC.2014.7032633.

[18] A. Singh, S. Mishra, and A. N. Tiwari, "Analysis of Improved power quality of Different types of Buck-Boost Converters with Power Factor Correction," *Int. Conf. Electr. Electron. Eng. ICE3 2020*, pp. 548–553, 2020, doi: 10.1109/ICE348803.2020.9122788.

[19] C. P. Tung, H. S. H. Chung, and K. K. F. Yuen, "Boost-Type Power Factor Corrector with Power Semiconductor Filter for Input Current Shaping," *IEEE Trans. Power Electron.*, vol. 32, no. 11, pp. 8293–8311, 2017, doi: 10.1109/TPEL.2017.2699038.

[20] J. G. Muñoz, "Análisis Dinámico y Control de un Convertidor Boost-Flyback,", Universidad Nacional de Colombia Sede Manizales Facultad de Ingeniería y Arquitectura Departamento de Ingeniería Eléctrica, Electrónica y Computación, 2017.